Pergamon

Int. J. Heat Mass Transfer. Vol. 40, No. 12, pp. 2785–2797, 1997

Printed in Great Britain
0017–9310/97 $17.00+0.00

PII: S0017–9310(96)00346–8

Electrochemical mass transfer measurements in rough surface pipe flow: geometrically similar V-shaped grooves

W. ZHAO and O. TRASS†

Department of Chemical Engineering and Applied Chemistry, University of Toronto, Ontario, Canada M5S 3E5

(*Received* 20 *December* 1995 *and in final form* 23 *September* 1996)

Abstract—The electrochemical technique has been used to measure mass transfer rates between nickel surfaces and the ferro-, ferricyanide electrolyte solution flowing in a 38 mm ID circular pipe. Data for one smooth and six rough surfaces are reported. The surfaces were fabricated by a novel electroplating technique. The rough surfaces had V-shaped grooves transverse to the flow direction, 76–1500 μm deep. The experiments covered the Reynolds number range of 500–350 000; Schmidt numbers varied from 550 to 4720. Friction factors were measured for $4000 < Re < 240\,000$. The results are correlated by the mass transfer similarity function. Transfer enhancement depends on groove size and frequency and on flow conditions. Rates higher than three times the corresponding smooth surface values were observed. A mass transfer efficiency index is proposed, relating enhancement to frictional losses. © 1997 Elsevier Science Ltd.

INTRODUCTION

Surface roughness plays an important role in fluid mechanics, heat transfer and mass transfer. While the effect of roughness on the first two has been studied thoroughly, relatively little work has been done on mass transfer. Yet, the effect can be significantly greater, particularly in high Schmidt number systems.

The classical pressure drop measurements of Nikuradse [1] for sand-roughened surfaces form the basis of the study of roughness effects on momentum transfer. As long as the surface is "hydraulically smooth", i.e. has a dimensionless roughness height, e^+ of less than five, there is no effect of roughness on pressure drop; as the roughness height increases, its influence on friction also increases and, finally, a "fully rough" condition or region is reached where the friction factor becomes independent of the Reynolds number. Nikuradse has also proposed the "roughness similarity function" $f(e^+)$ which varies linearly with $\log(e^+)$ in the smooth region, goes through a maximum in the "transition" region and levels off at a constant value of 8.48 in the fully rough region. This function correlates all the frictional resistance data well, for all roughness sizes and all Reynolds numbers.

For heat transfer, Dipprey and Sabersky [2] have extended Nikuradse's approach to heat transfer and proposed the "heat transfer similarity function", $g(e^+, Pr)$. It brings in the Prandtl number as an additional parameter and, just as Nikuradse's work, is limited to geometrically similar surface roughnesses of different sizes.

The work of Dawson on mass transfer at rough surfaces [3, 4] resulted in the development of the mass transfer similarity function, $g'(e^+, Sc)$, again for geometrically similar surfaces. Tantirige and Trass [5] extended the results to different pitch-to-height ratios. The rectangular 25 × 25 mm test section used in their work, with the rough surface covering only the central portion of one wall, made the measurement of pressure drop difficult. Also, mass transfer measurements were influenced by entrance and edge effects as well as by secondary flows in the square duct.

To eliminate these disadvantages, the measurements reported here were carried out in round pipes. The data can then be compared more readily with, and incorporated in, the large data base on momentum and heat transfer results available in the literature for pipe flows. Getting regular roughnesses on the inside wall of a relatively long pipe section posed its own problems, however. The technique finally adopted for making the rough nickel surfaces required for electrochemical mass transfer measurements is described next.

EXPERIMENTAL

Rough surface electrodes

Machining of rough surface electrodes on the inside pipe wall is extremely difficult, even for short lengths. The method adopted involves four steps. First, the mirror image of the desired pattern is machined on the outside of an aluminium pipe. Nickel is then elec-

† Author to whom correspondence should be addressed.

NOMENCLATURE

A	cathode area, projected [m^2]
C_b	bulk concentration [mol m^{-3}]
D	diffusion coefficient [m^2 s^{-1}]
d	diameter [m]
e	roughness height [m]
e^+	roughness Reynold number eu^*/ν
f	friction factor
F	Faraday constant
$g(e^+, Pr)$	heat transfer similarity function
$g'(e^+, Sc)$	mass transfer similarity function
I	cell current [A]
I_{lim}	limiting cell current [A]
k	mass transfer coefficient [m s^{-1}]
L	length of the cathode [m]
p	pitch (roughness spacing) [m]
Pr	Prandtl number [ν/α]
Re	Reynolds number (dU/ν)
Sc	Schmidt number (ν/D)
Sh	Sherwood number (kd/D)
St	Stanton number ($Sh/ReSc$)
u^*	friction velocity [m s^{-1}]
U	average velocity [m s^{-1}]
y	distance from wall [m]
y^+	dimensionless distance from wall (yu^*/ν)
Z	valence change.

Greek symbols

α	thermal diffusivity [m^2 s^{-1}]
ΔP	pressure drop [Pascals]
ν	kinematic viscosity [m^2 s^{-1}]
ρ	density [kg m^{-3}].

Subscripts

R	rough surface
S	smooth surface.

troplated onto that pattern, to create a perfect reproduction, in a specially-designed plating bath shown in Fig. 1(a). The nickel coating must be thick enough to be also the structural component of the pipe, typically 2–3 mm. The aluminium pipe is then dissolved in strong caustic solution. Finally, a flange arrangement is made to fit the nickel test section into the main flow loop. A smooth transition must be provided so as to minimize flow disturbances.

The electrolyte solution in the plating bath contained 4 M soluble nickel sulfamate, $Ni(NH_2SO_3)_2$ and 1M boric acid which acted as a buffer to maintain the pH around five. A small amount of surfactant was added to prevent hydrogen bubbles from attaching to the cathode surface. The aluminium pipe was the cathode shown in Fig. 1(a). The anode comprised four baskets of S-round nickel from INCO Ltd.

Plating was started at the low voltage of 0.6 V giving a low current; after about 36 h voltage was increased to 1 V and after a further 48 h to 2.5 V for more rapid nickel buildup, with the air sparger turned on at that time. It took, typically, 10–14 days to plate a good surface. After dissolution of the aluminium pipe, a dark layer (of unknown composition) was observed on the fresh nickel surface. A mixture of 1M HCl and about 1% hydrogen peroxide removed the dark matter within a few minutes. Further details are given in ref. [6].

The roughnesses made were triangular grooves around the periphery of the 38 mm inside diameter tube. The grooves on the rough surfaces for which data are reported here, were to have a 60° bottom angle and a pitch-to-depth (roughness height) ratio, p/e, of five. The three largest roughnesses, called R1, R2 and R5, met those criteria. For the smaller roughnesses R7 and R8, machining had not been precise and both the angle and the depth deviated from expectation. The numbering system for the surfaces used in ref. [6] is retained here. The characteristic dimensions are given in Table 1 and the actual shapes are sketched in Fig. 1(b), on the same scale, for surfaces R5–R8. R1 and R2 are larger than R5 by factors of three and two, respectively, but identical in shape. Surface R6 is included, as it is used for some comparative comments later. It represents surfaces with a lower p/e ratio. All surfaces are 30 cm in length.

The electrochemical technique

The electrochemical technique used in mass transfer studies involves the measurement of the current flowing in an electrochemical cell, operating under conditions such that the reaction rate is diffusion controlled and ionic migration is negligible. The popular ferro-, ferricyanide system in a sodium hydroxide solution was used. When a voltage difference is imposed across the electrodes, the following reaction occurs at the cathode

$$Fe(CN)_6^{3} + e \rightarrow Fe(CN)_6^{4}$$

with the reverse reaction at the anode. Thus, the composition of the electrolyte solution does not change. A high concentration of sodium hydroxide maintains a high conductivity, thus eliminating migration effects. It also allows control of the Schmidt number, as diffusivity and viscosity depend on both temperature and NaOH concentration.

The cathode was used as the controlling electrode so that ferricyanide ion diffusion controlled the current. At the cathode surface, concentration is zero. Thus the mass transfer coefficient k is related to the limiting current I_{lim} by

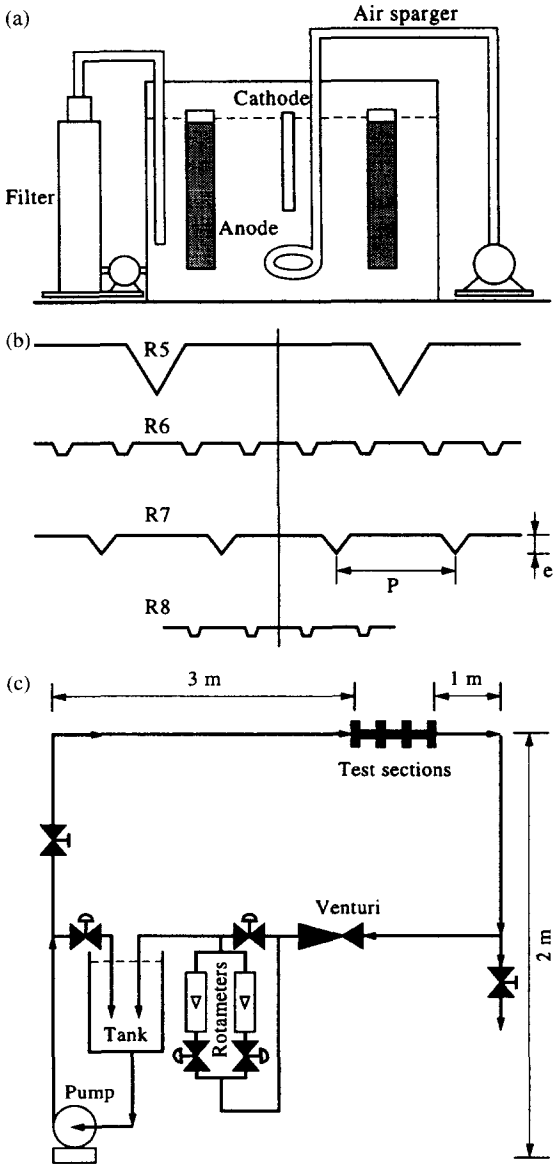

Fig. 1. Schematic diagrams of: (a) the plating tank; (b) profiles of surfaces R5–R8; and (c) flow system.

$$k = I_{\text{lim}}/ZFAC_b \qquad (1)$$

where Z is the valency change in the reaction, F Faraday's constant, A the projected area of the cathode and C_b the bulk concentration of the reacting species.

In systems where mass flux is high, proper preparation of the cathode surface is necessary to ensure that the whole surface is active and that the reaction rate will not be the controlling factor. It was found that 4 min of cathodic treatment of the rough surfaces in 1–1.5 M sulfuric acid electrolysis cell resulted in good, reproducible polarization curves and a constant value of I_{lim}/C_b.

Flow-loop and experimental procedure

The experimental set-up shown in Fig. 1(c) formed a closed loop from the 3 HP centrifugal pump through PVC pipe with an internal diameter of 38 mm, to the nickel test section, a venturi flow meter, two rotameters (when needed) and a 200 l polyethylene tank. The low flow rate range was measured by one of two small rotameters, the intermediate range by larger rotameters or the venturi and the highest, by the venturi meter with a mercury manometer used to measure the pressure difference. An inverter was used to adjust the RPM of the pump motor and hence to control the flow rate. A bypass loop was provided but used only to prepare the solution. Nitrogen was bubbled through the solution to deoxygenate it prior to the start of an experiment. During an experimental run, the system was first brought to the desired operating temperature with steam, hot water or cooling water; polarization curves were checked at various flow rates and their midpoints used to set the operating voltages at which the limiting current measurements were taken over the whole range of flow rates suitable for the particular solution concentration. The electrical circuit was conventional and is given, along with many other details, in ref. [6].

Figure 2 illustrates polarization curves obtained at high Reynolds numbers. A wide polarized region was achieved even at a Reynolds number of 347 000 by reducing the concentration of the reacting cyanide ions, as well as using two anodes, one upstream and one downstream of the cathode. This is the highest value reported in the literature for diffusion control and was obtained when the electrolyte composition was: 0.001 M or 0.00025 M $K_3Fe(CN)_6$, 0.005 M $K_4Fe(CN)_6$ and 1 M NaOH in water. For low Reynolds numbers only the downstream anode was used.

In addition to mass transfer measurements, the friction factor was determined for all surfaces from pres-

Table 1. Rough surface characteristics

Surface	Pitch, p (mm)	Depth, e (mm)	Angle, θ (degrees)	p/e actual	p/e intended
R1	7.5	1.5	60	5	5
R2	5.0	1.0	60	5	5
R5	2.5	0.50	60	5	5
R6	0.62	0.154	70	4	2.5
R7	1.25	0.173	70	7	5
R8	0.62	0.076	51	8	5

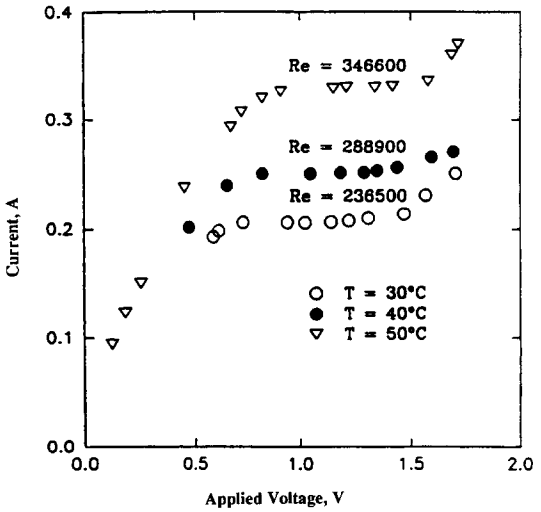

Fig. 2. Polarization curves for surface R2.

sure drop measurements. Two pressure transducers and a mercury manometer were used to cover the nearly 3000-fold range of pressure drop values. Pressure taps must be inserted with great care and their reliability tested over the range of flow rates to obtain accurate results.

With an approach length of 3 m of smooth pipe, Fig. 1(c), flow was fully developed. The effect of roughness started with the 30 cm test section, however. Similarly, mass transfer starts there, so the results, averaged over the length of the cathode, include an entrance effect.

RESULTS AND DISCUSSION

Mass transfer in the smooth pipe

Data obtained in the smooth pipe at the four Schmidt numbers used ($550 \leqslant Sc \leqslant 4720$) are presented in Fig. 3 over the full range of Reynolds numbers, covering the laminar, transitional and turbulent flow regimes, from $Re = 500$ to $Re = 350\,000$. The mass transfer coefficient is made dimensionless by representing it as a Sherwood number, Sh. Overlap of multiple points here and in other figures indicates usually overlap regions when cyanide concentration was changed. Generally good data consistency and reproducibility are indicated. Separate error analysis of both Sh and Re values also suggests that the size of symbols used is a reasonable representation of the potential measurement errors.

The turbulent flow data at $Re > 10\,000$ are correlated with a standard deviation of 3% by

$$Sh = 0.013\, Re^{0.88} Sc^{0.32}. \quad (2)$$

The exponents are the same as reported by Dawson and Trass [4] and agree well with the exponents predicted by Lin *et al.* [7], 7/8 and 1/3, respectively. Dawson's data are higher due to the aforementioned limitation of his square duct geometry, i.e. edge and side effects. With a fully developed concentration boundary layer, a slightly lower rate than given in equation (2) would be expected, as for the 30.5 cm long cathode ($L/d = 8$) the entrance length effect cannot be ignored.

The laminar data ($Re < 3000$) are represented by

$$Sh = 2.14(Re.Sc.d/L)^{1/3} \quad (3)$$

and show, as expected, a strong effect on cathode length, in agreement with the results of Pickett and Ong [8]. It should be noted that the exponent on the Schmidt number is the same for both laminar and turbulent conditions.

The emphasis in this paper will be on turbulent transfer. Interesting observations made at low Reynolds numbers and large roughness elements [6] will be presented in a subsequent publication. The data just shown provide the smooth surface values for all subsequent comparisons.

Mass transfer at rough surfaces

Mass transfer regimes for rough pipes differ significantly from those for smooth pipes; the size of roughness also matters. This is illustrated in Fig. 4. The Sherwood number results reported there and subsequently are all based on the projected surface area, i.e. the same as the area of the smooth surface, average for the 30 cm long surfaces.

In Fig. 4(a), for the highest roughness, surface R1, at all four Schmidt numbers, four distinct regions are observed: laminar, below $Re \simeq 2000$ where the data are parallel to but higher than the smooth surface value; transition to turbulent transfer between $Re = 2000$ and 4000 with a very steep rise of the Sherwood number (multiple values at the same Re differ significantly); followed by a wide region where Sh grows at a slower rate than the smooth surface value (only $Sc = 550$ lines drawn), i.e. the slope is lower, to $Re \simeq 50\,000$–$70\,000$; and finally, the data points become parallel to the smooth surface values, i.e. the ratio Sh_R/Sh_S does not change further. One might suggest that in the last region any effect of the roughness elements on turbulence near the surface is fully developed.

Figure 4(b), for surface R7, with the second smallest roughness also shows four regions: the first, laminar, as before; then transition to turbulent flow occurs but the data coincide with the smooth surface results (again seen most readily for $Sc = 550$ for which smooth lines are drawn); then, starting at $Re = 15\,000$, the smooth surface data are left behind and the Sh values rise rapidly—the first effect of surface roughness; somewhere around $Re \simeq 50\,000$–$80\,000$, the data become parallel with the smooth surface line and then fall just slightly with respect to the smooth data.

Before leaving these graphs, the effect of the Schmidt number should be reported. For the two last

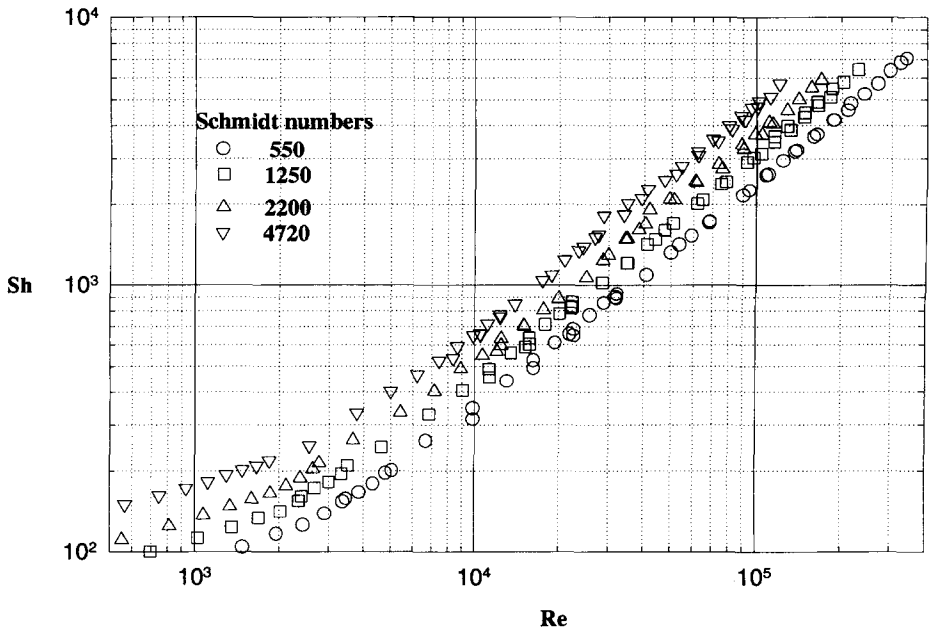

Fig. 3. Sherwood number vs Reynolds number, smooth surface.

regions for surface R1, the results may be correlated by

$$Sh = 0.134\, Re^{0.68} Sc^{0.39} \quad 6000 \leqslant Re \leqslant 60\,000$$
$$500 \leqslant Sc \leqslant 5000 \tag{4}$$

and

$$Sh = 0.012\, Re^{0.88} Sc^{0.39} \quad Re \geqslant 60\,000$$
$$500 \leqslant Sc \leqslant 5000 \tag{5}$$

respectively. In the rapid rise phase the relationship is more complicated; the Schmidt number exponent increases from 0.32 to 0.39. For surface R7 in the last region, the correlation is

$$Sh = 0.03\, Re^{0.79} Sc^{0.45} \quad Re \geqslant 60\,000$$
$$500 \leqslant Sc \leqslant 5000. \tag{6}$$

The exponent on Re is below 0.88, confirming the lower slope observed and the Schmidt number effect is again different. In the rapid rise region, the Schmidt number exponent has to change from 0.32 to 0.45; spreading of the data points in the vertical direction is apparent in the figure. Reported literature values [4, 9] are 0.41 and 0.43. For heat transfer at rough surfaces, Prandtl number exponents from 0.43 to 0.56 has been reported [2, 10, 11], all for the substantially developed roughness effects corresponding to those here.

These results show that, in addition to the Schmidt number effect, large roughness elements may already influence laminar transfer (by both the increased surface area and by flow disturbances) and that their effect becomes dominant already in the normal transition region from laminar to turbulent flow. Surfaces with the small roughness elements behave as if they were smooth well into the turbulent flow regime; their roughness characteristics show up only after they emerge from the hydraulically smooth condition. They then cause a rapid increase in the rate of mass transfer and, depending on their size and the Reynolds number range covered, reach one or both of the regimes characteristic for high Reynolds numbers and large roughness elements.

Next, for the highest Schmidt number of 4720 only, results for all five more-or-less similarly rough surfaces are shown, again as Sh vs Re, in Fig. 5. Three of the six curves on this busy figure are already familiar to the reader; the others are seen to fall in line in the expected order. The Sherwood number for surfaces R1 and R2 (substantially overlapping) rises first, R5 next makes its move, starting at $Re \simeq 4000$, followed by R7 at $Re \simeq 7000$ and R8 at $Re \simeq 20\,000$.

Rough-to-smooth transfer ratio

Before turning our attention to the mass transfer similarity function, it is instructive to look at the ratios of rough-to-smooth surface transfer coefficients, i.e. Sh_R/Sh_S. This ratio is plotted for the five rough surfaces against the Reynolds number in Fig. 6, again for $Sc = 4720$. Here, the ordinate scale is expanded considerably, thus allowing finer distinctions to be observed. For example, surfaces R1 and R2 rise together but no longer overlap at the higher Reynolds numbers. R5 matches the smooth surface data up to $Re = 2000$, then rises, with the steepest rise over $3000 < Re < 10\,000$. The two sets of overlapping R5 data at $Re = 6000$–$11\,000$ and again at $Re \simeq 20\,000$–$35\,000$ illustrate changes in solution concentrations

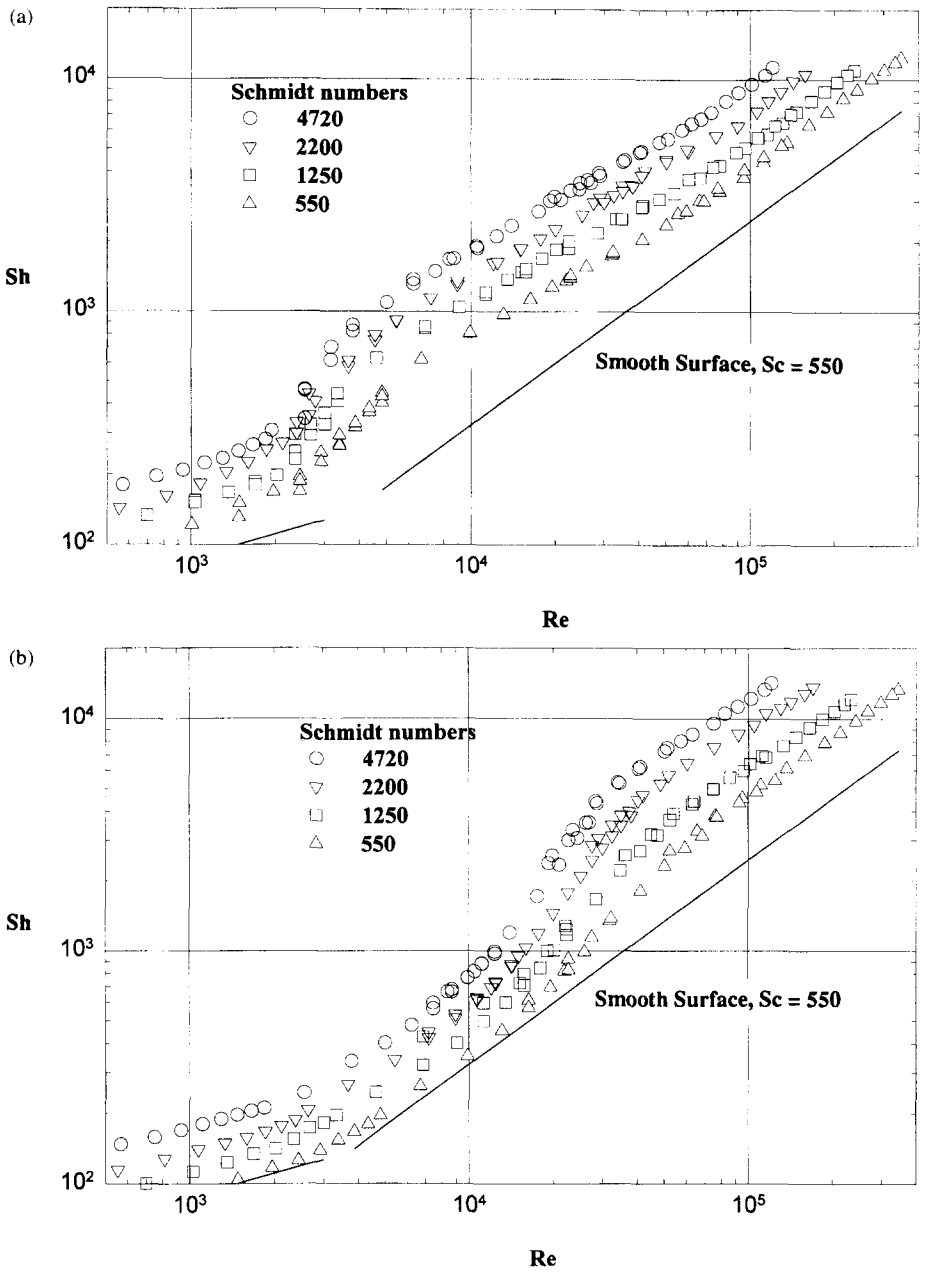

Fig. 4. Sherwood number vs Reynolds number: (a) surface R1; and (b) surface R7.

and give a good measure of the reliability of the individual data sets, on this expanded scale.

Surfaces R7 and R8 rise at their respective higher Reynolds numbers and overshoot the larger roughness values at the highest Reynolds number. It is also apparent that R8 is just settling into a "developed" condition.

Friction factor data

Pressure drop measurements were made over a Reynolds number range from 4000 to 240 000, with water, for the smooth and all rough surfaces. Measurement ranges (and overlaps) were $Re = 4000$–$23\,000$, $Re = 13\,000$–$140\,000$ and $Re = 65\,000$–$240\,000$. The friction factors are calculated from measured pressure drop values using equation (7).

$$\Delta P_f = f \cdot \frac{L}{d} \frac{\rho U^2}{2}. \tag{7}$$

Results for the smooth surface are compared with the data of Nikuradse [1] and Dipprey and Sabersky [2] in Fig. 7. The well-known Blasius equation, valid for turbulent pipe flow up to $Re = 100\,000$

$$f = \frac{0.3164}{Re^{0.25}} \tag{8}$$

and the logarithmic equation proposed by Prandtl [12] for higher Reynolds numbers,

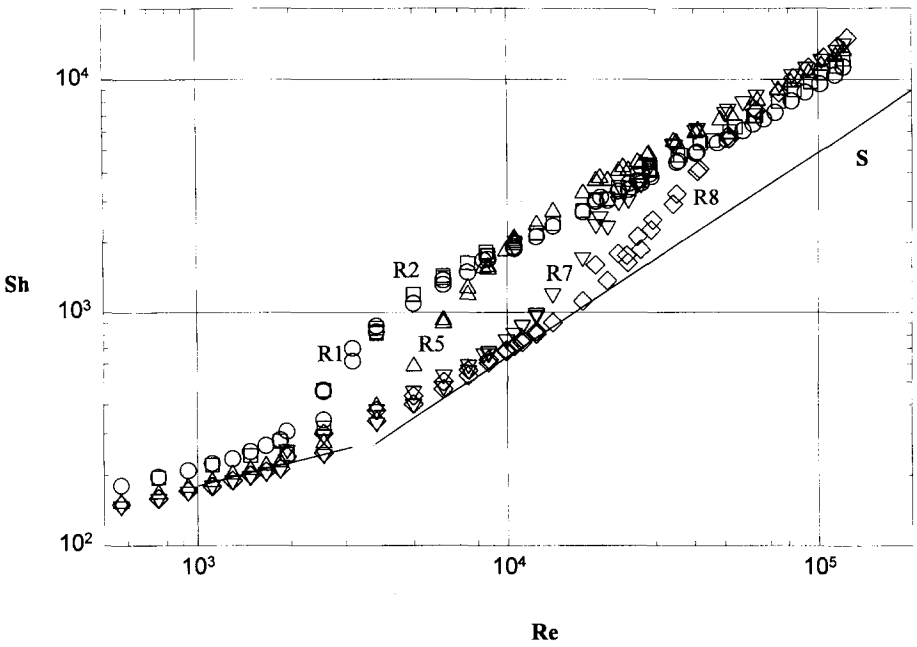

Fig. 5. Sherwood numbers vs Reynolds number, surfaces R1, R2, R5, R7 and R8; $Sc = 4720$.

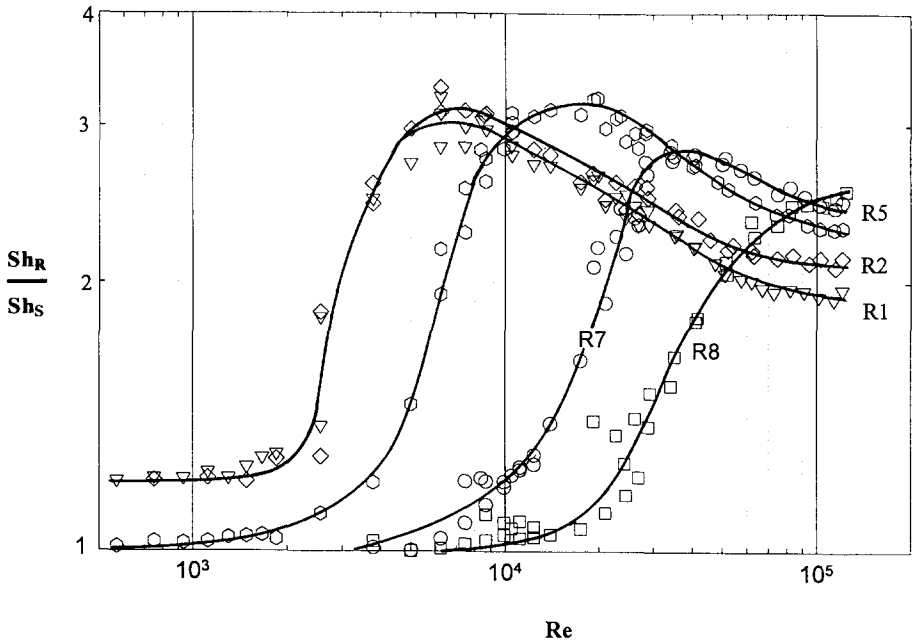

Fig. 6. Sherwood number ratio vs Reynolds number, surfaces R1, R2, R5, R7 and R8; $Sc = 4720$.

$$\frac{1}{\sqrt{f}} = 2.0\log(Re\sqrt{f}) - 0.8 \tag{9}$$

are also plotted, along with Poiseuille's law for laminar flow.

The friction factor results match the Blasius and Prandtl equations well, with a slight overshoot at the highest Reynolds number. The Nikuradse data are for a surface with a small roughness ($d/e \simeq 1000$); also the present one, nickel-plated as all the other surfaces, may not have been perfectly smooth.

Friction factors for the five rough surfaces and the smooth one are presented in Fig. 8. The largest roughness, R1, with 1.5 mm deep grooves, gives a lower resistance than R2 with 1.0 mm deep grooves. This was a surprise, but may be explained by realizing that these large roughnesses equal 8% of the pipe diameter and the frequency of roughness elements, at the same

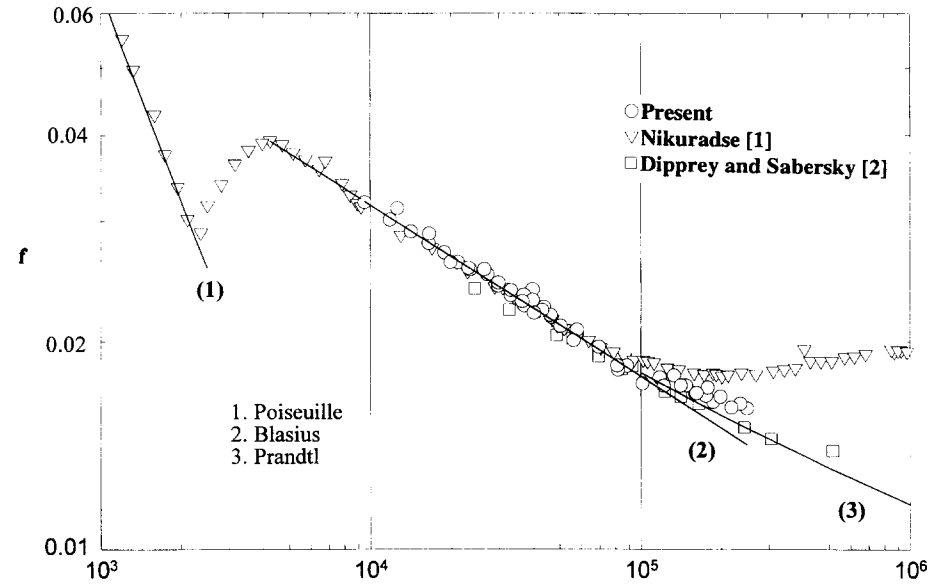

Fig. 7. Comparison of friction factor data at the smooth surface with the literature.

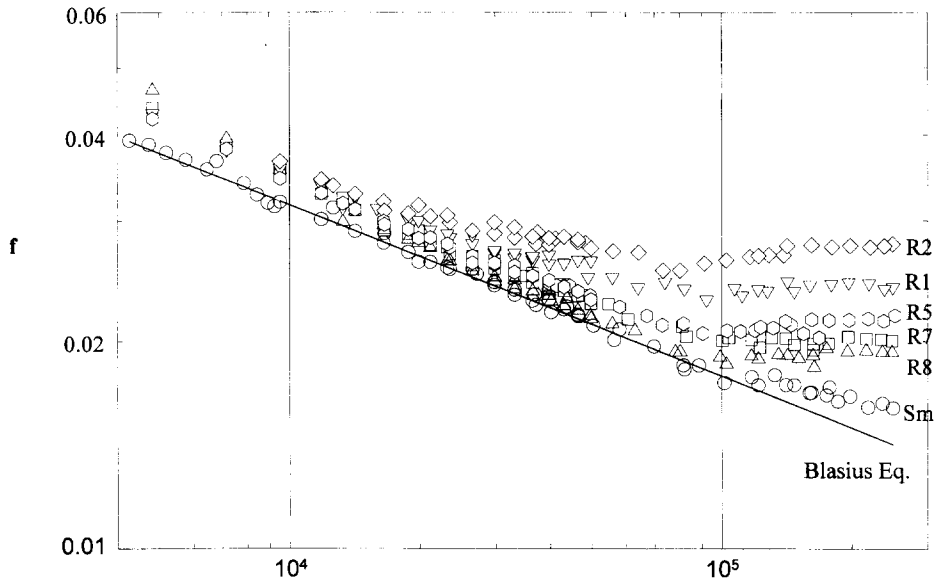

Fig. 8. Friction factor data, surfaces R1, R2, R5, R7 and R8.

$p/e = 5$ is, of course, lower. Their interaction with the flow, and generation of turbulence near the wall likely does not line up any more with the other geometrically similar rough surfaces; there is an upper limit to events occurring in the "region near the wall".

Starting with R2, all friction factors line up well with size, as do Nikuradse's and Dawson's. The trend, seen clearly with R2 and R5, of the friction factor attaining a minimum, e.g. at $Re = 90\,000$ for R5, then rising and finally levelling out (at $Re \simeq 160\,000$) to a constant value, has been observed by Nikuradse and others.

It would be interesting to consider here the friction factor results correlated in terms of the friction similarity function. However, to focus attention on the mass transfer results, this too will be left for a future publication. The analysed results are available in ref. [6].

Mass transfer similarity function

In order to evaluate the mass transfer similarity function, it is necessary to find the dimensionless roughness height, e^+, also called the roughness Reynolds number.

$$e^+ = \frac{u^* e}{\nu} \tag{10}$$

where u^* is the friction velocity obtained from the friction factor,

$$u^* = U\sqrt{f/8}. \tag{11}$$

The variable e^+ incorporates both independent variables; velocity or Reynolds number and roughness size. For protruding roughness elements, e^+ can be readily referred to as the dimensionless distance y^+ (distance y from the wall replacing e in equation (10)) to ascertain the extent of their protrusion into the boundary layer. For roughness elements such as grooves below the flat wall, it may be simplest to think about e^+ also as a measure of turbulence intensity in the grooves, i.e. to relate it qualitatively to near-wall turbulence structures through which mass transfer is enhanced.

Dawson and Trass [4] showed that for high Schmidt numbers the mass transfer similarity function is reduced to the ratio of rough to smooth surface transfer coefficients, or

$$g'(e^+, Sc) = \frac{Sh_R}{Sh_S} = \frac{St_R}{St_S} = \frac{k_R}{k_S}. \tag{12}$$

As the function g' depends on surface geometry so does the Sherwood or Stanton number ratio (the latter has been used in several publications). With their data, a good correlation was obtained for $e^+ > 25$. An additional limit is imposed for large roughnesses by the "law of the wall" assumption which breaks down at low Reynolds numbers. The coarser roughnesses deviated from the simple correlation at $Re \simeq 15$–20 000. For the smallest roughnesses, the function becomes more complex at $e^+ < 25$, but should hold. Their correlation for $e^+ > 25$ is

$$\frac{Sh_R}{Sh_S} = 1.94\, Sc^{0.09}(e^+)^{-0.10} \tag{13}$$

for etched grooves, between V and U shapes with $p/e \simeq 3.75$.

Figure 9 gives the Sh_R/Sh_S results plotted against e^+. It is observed that there is considerable compaction of the data. All surfaces display a ratio close to unity for $e^+ \leqslant 2$, where the surfaces are hydraulically smooth. From $3 < e^+ < 10$, there is a rapid rise in the Sh_R/Sh_S ratio which peaks at $e^+ \simeq 10$–15, then declines and eventually reaches constant values for the large roughnesses. The results of Dawson and Trass [4] at $Sc = 4590$, close to the 4720 used here, fit into the envelope between the dashed lines. The proper similarity function should follow the lower of the envelope curves, corresponding to the finer and finest surface roughnesses still at sufficiently high Reynolds numbers. Those results rise a little earlier and a little higher, to be expected for the more frequent roughness elements used in that study [see also further comment re. Fig. 11(b)]. The e^+ range here is an order of magnitude greater; the general trend of the data follows that reported by Dawson and Trass [4]. The wide range of Reynolds numbers over which these events occurred previously is now quite compact in terms of e^+, the roughness Reynolds number.

Taking all the data, that is, also at the other three Schmidt numbers (not shown here) into consideration, one observes that the "hydraulically smooth" region is stretched from $e^+ \simeq 2$ at $Sc = 4720$ to $e^+ \simeq 3$ at $Sc = 2200$ and $e^+ \simeq 4$ at $Sc = 550$ [6], not surprisingly. Since the low rate of molecular diffusion very near the wall is the major resistance to mass transfer, any induced turbulence which reaches the wall is expected to cause a greater increase in mass transfer rates in lower diffusivity, or higher Schmidt number, systems. Thus, even the tiniest amount of turbulence has an effect when the Schmidt number is high enough. This explains both the earlier rise and the higher peak ratios observed at the higher Schmidt numbers, both here and by Dawson and Trass [4]. For surfaces R1, R2 and R5 only, which all extend to sufficiently large e^+ values, the data beyond the peak, that is in the declining region, can be correlated by

$$\frac{Sh_R}{Sh_S} = 1.79\, Sc^{0.12}(e^+)^{-0.17}. \tag{14}$$

Compared to equation (13), the Schmidt number exponent is slightly higher and the rate of decline rather steeper than that observed by Dawson and Trass [4] for their rough surfaces. There is no reason to expect the e^+ exponent to be the same, as it depends on surface geometry. The Schmidt number dependence may, however, be expected to be substantially similar.

Grimanis and Abedian [9], in a more limited study report for their three geometrically similar surfaces (judged from friction behaviour) in the fully rough region

$$\frac{Sh_R}{Sh_S} = 2.0\, Sc^{0.1}(e^+)^{-0.2}. \tag{15}$$

The Schmidt number exponent fits closely and the ratio drops off even faster with e^+ than observed in this study.

Mass transfer efficiency index

It may often be desirable to enhance the mass transfer rate and to do so at a minimal cost. The cost here is pressure drop. Therefore, to compare the relative advantage of different rough surfaces for such mass transfer enhancement, the "mass transfer efficiency index" has been defined as the ratio of transfer coefficient to friction factor enhancement, $(Sh_R/Sh_S)/(f_R/f_S)$. Figure 10 gives this index plotted against the

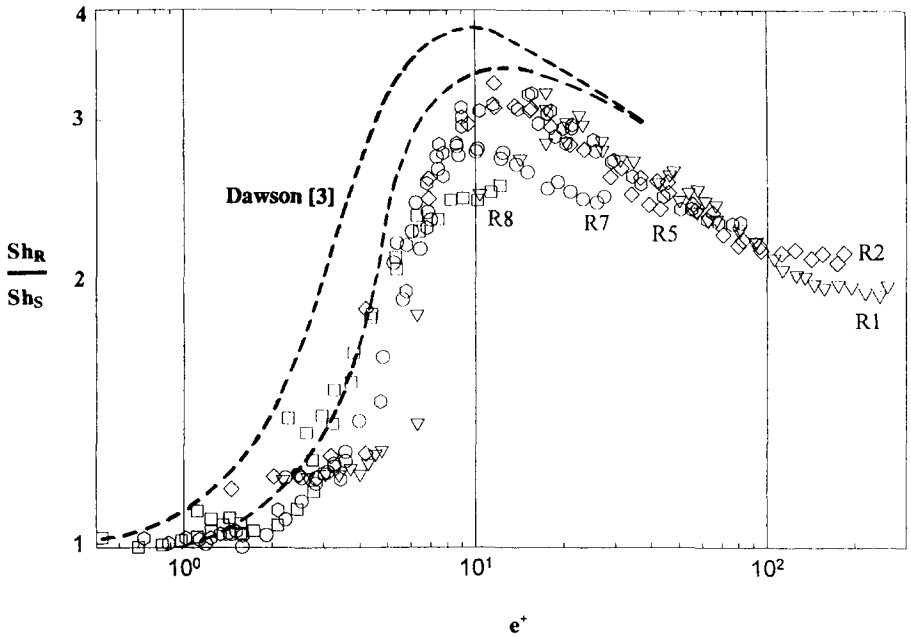

Fig. 9. Sherwood number ratio vs e^+, surfaces R1, R2, R5, R7 and R8; $Sc = 4720$.

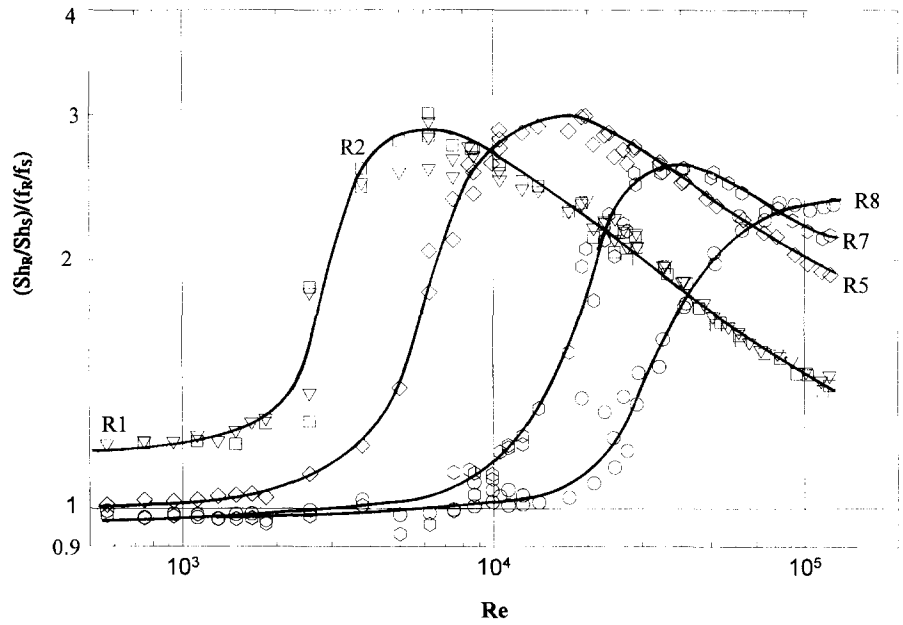

Fig. 10. Mass transfer efficiency index vs Reynolds number, surfaces R1, R2, R5, R7 and R8; $Sc = 4720$.

Reynolds number for the five geometrically similar rough surfaces, at $Sc = 4720$. The trends are not too different from those shown in Fig. 6 without division with the friction factor ratio. All numbers are, of course, a little lower.

It is apparent that at low Reynolds numbers, below 10 000, surfaces R1 and R2 do the best. Their small difference observed in Fig. 6 has been cancelled out by the friction factor variation and they are quite indistinguishable. For $Re > 10\,000$, R5 is best but then drops off and is replaced by R7 at $Re \simeq 40\,000$ which in turn must yield to R8 at $Re > 90\,000$. In other words, the higher the Reynolds number range of interest, the finer a surface roughness one would wish to use. None of these regularly rough surfaces does well over a wide Reynolds number range.

Also these data could be compressed into a better correlation when plotted against e^+, but little would be gained here. This important point is made with greater clarity in terms of the familiar Reynolds number.

Since in the last several figures data only at the highest Schmidt number have been shown, Fig. 11(a) gives the efficiency index for surface R5 also at

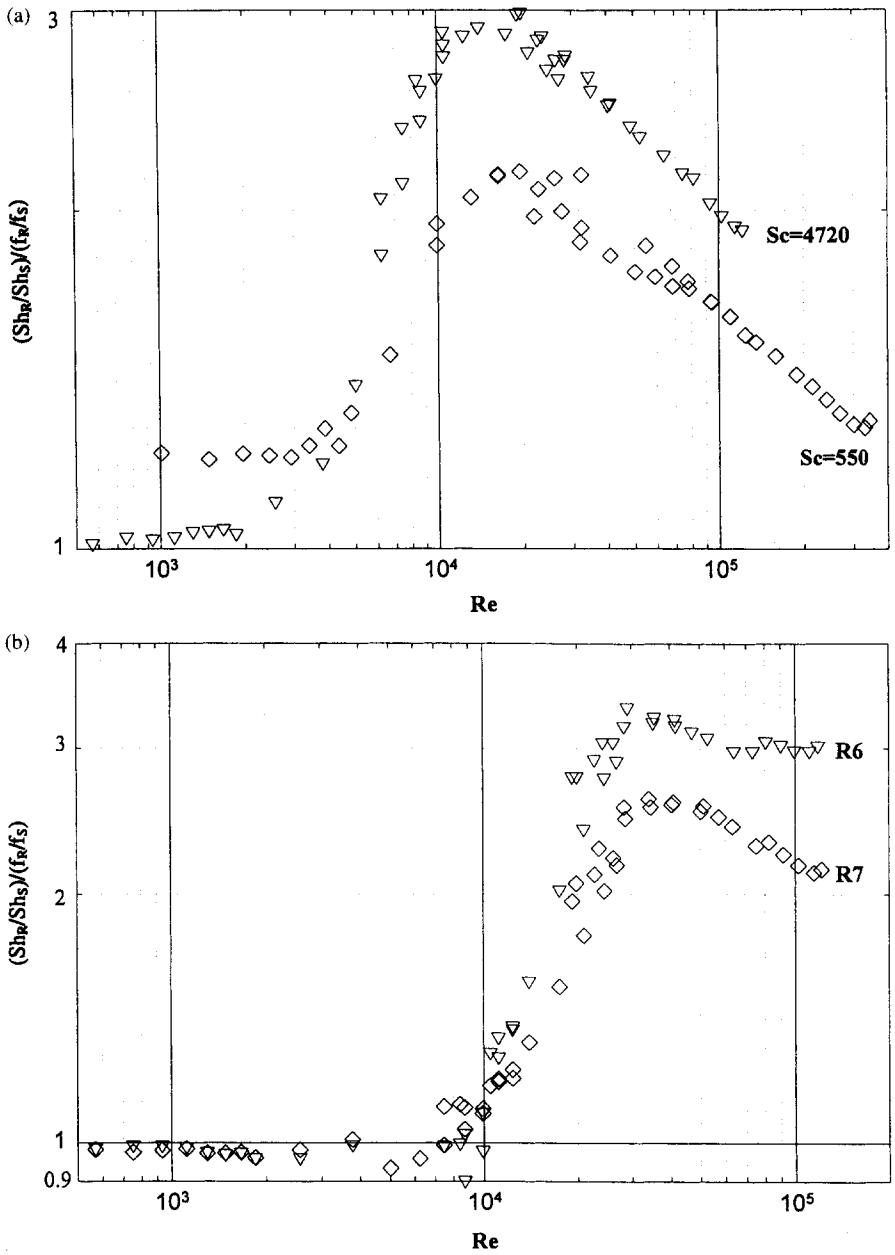

Fig. 11. Mass transfer efficiency index vs Reynolds number; (a) surface R5; $Sc = 4720$ and 550; and (b) surfaces R6 and R7; $Sc = 4720$.

$Sc = 550$. We observe here and would observe for all other surfaces, that the index is considerably lower—the peak is shifted to a slightly higher Re value, but reduced by over 25%. Intermediate values spread as would be expected. Due to the lower viscosity of the higher temperature, lower NaOH concentration solution required to have the lowest Schmidt number, the highest Reynolds number, 350 000, was attained.

Further comments

It may be tempting to start to draw conclusions from the data given above. Yet, other information, some of it hard to explain, must temper that temptation. For different p/e ratios, Tantirige and Trass [5] found that a higher frequency of elements, i.e. lower p/e ratio, gave generally higher mass transfer rate enhancements. The same is true here.

Figure 11(b) presents the efficiency index for surface R7 along with that of R6 with substantially the same groove dimensions (only a little shallower, 0.154 vs 0.173 mm depth) but with twice as many grooves per unit length of cathode surface. The p/e value for R7 is 7 and for R6 it is 4; both have an angle of 70° (see Table 1). The friction factor for R6 is higher than that for R7, just above R5, but the Sherwood number more than makes up for that, resulting in the considerably

higher efficiency index. Both start to rise at $Re \simeq 8000$–$10\,000$ and R6 stays slightly ahead of R7. Also, that observation in confirmed qualitatively in ref. [5]. Surface R6 happens to be quite similar to one of Dawson's surfaces (the latter have a comparable angle of 83°); aside from a small difference in the rise region, mass transfer enhancements in the fully developed region virtually coincide.

Values of the mass transfer efficiency index observed here are mostly in the range of 2–3, with the peaks of the Sherwood number ratio slightly higher. Comparable peak values at the high Schmidt numbers reported in refs. [4] and [5] are in the range of 3–4, close to the peak value of R6 at 3.8. As pointed out earlier, that shift is mainly caused by the higher frequency of roughness elements used in those studies.

In heat transfer work, often a comparable transfer efficiency index would be close to or below one. Webb *et al.* [10] show, for ribbed roughness, indices from 0.2 to 1.6, increasing as the Prandtl number is increased. The index is around 0.6 at $Pr = 1$, unity at $Pr = 10$ and 1.6 at $Pr = 100$. An extension of such a trend to higher transport property numbers, all the way to our Schmidt number values, would reasonably suggest an index value of 2–2.5 at $Sc \simeq 500$ and 3–4 at $Sc \simeq 5\,000$.

These numbers are quoted here to suggest that there is a certain measure of unity in heat and mass transfer work and corresponding heat transfer values could be estimated from the work presented here. Indeed, as part of a future collaborative project both heat and mass transfer data will be obtained for the same rough surfaces, to provide definitive confirmation of such estimates.

It is clear that great caution must be exercised when considering heat-mass-momentum transfer analogies for flow past rough surfaces. Form drag does not have a counterpart in heat or mass transfer since neither heat nor mass are vector quantities while momentum is. Analogous behaviour for heat and mass transfer can, for the same reason, be invoked with a much greater degree of certainty.

Composite surface

It is apparent that the best mass transfer enhancement is attained at e^+ values of 10–15. On a Reynolds number scale, the same e^+ corresponds to different roughness sizes at different Reynolds numbers, in some proportion to the wall-region thickness of the boundary layer. Thus, for any specific condition, a plausible roughness pattern may be recommended. If it is desired, however, to have one surface enhance mass transfer for a broad range of flow conditions, some composite structure may be called for. For randomly rough, three-dimensional (3-D) surfaces, obtained by sintering nickel powder onto a nickel plate, transfer enhancements up to twice those reported here, i.e. in the 6–8 range have been reported [13]. With that information in mind, a surface with a regular, relatively large roughness pattern may be suggested, in combination with a superimposed random, 3-D roughness of smaller scale.

One other observation: surfaces R3 and R4 in the present series [6] have the same depth as R2, 1 mm, the same p/e value, but different angles, 90°C and 120°C compared to 60°C for R2. The mass transfer performance is virtually identical yet, friction factors are dramatically different, with the highest angle giving the greatest pressure drop. Those surprising results, along with a greater emphasis on friction behaviour of surfaces will be the subject of a forthcoming publication.

Future work

In order to gain a better understanding and to form an improved conceptual model of the phenomena at regularly rough surfaces, it is essential to study the fluid flow patterns at such surfaces so as to better understand first the momentum transfer phenomena. Obviously very different wall-region flow patterns (e.g. at R2 vs R4) can give the same mass transfer results. Local mass transfer rates may, of course, be quite different, reflecting the different flow phenomena, yet give the same average result. Indeed, for adequate understanding, one will also have to study local transients—both turbulent flow phenomena, i.e. the instantaneous turbulence structures and the corresponding mass transfer rate variations.

We do have the tools to do that. An early attempt is described in ref. [14] where some flow phenomena in and above single V-shaped grooves have been reported. Current flow visualization techniques as further developed at the University of Toronto now allow detailed flow patterns to be observed and quantified, with surprisingly fine resolution [15]. That novel technology must next be utilized to attack first the flow problem. Then the question of local mass transfer at surface roughness elements arises. One approach which can be taken is the use of local spot electrodes. It has been pioneered by Reiss and Hanratty [16] and allows measurements at selected positions. Other possible approaches, to allow more continuous measurements are also being considered. Only after those steps have been taken will further analysis and building of a meaningful conceptual/mechanistic model of the phenomena be possible. It is then appropriate also to reanalyze the currently available data, with much greater understanding.

The study of turbulent bursts at smooth surfaces pioneered by Kline and his group [17] has shown that momentum transfer for turbulent conditions near the wall takes place largely by such bursts. The occurrence of similar bursts at surface roughness elements, actually easier to visualize than at smooth surfaces, has been confirmed by Tantirige *et al.* [14]. Such bursts which cause rapid exchange of liquid near the surface, the inside of cavities included, likely provide also the main mechanism for mass transfer enhancement by surface roughness. Once that picture emerges, our knowledge of transport phenomena at rough surfaces

will have been considerably enhanced and interpretation of the data reported here and elsewhere will become a much easier task. We will then also be in a good position to predict performance and to design better surface structures for the enhancement of heat and mass transfer rates.

SUMMARY AND CONCLUSIONS

Mass transfer coefficients have been measured for a smooth and a series of five geometrically similar V-grooved roughness elements inside a 38 mm pipe using the electrochemical technique. Wide ranges of Schmidt and Reynolds numbers were covered, $550 \leqslant Sc \leqslant 4720$ and $500 \leqslant Re \leqslant 350\,000$. Friction factors for these surface were also measured, over the range $4000 \leqslant Re \leqslant 240\,000$. Thus the roughness Reynolds number e^+ could be calculated for each surface and flow condition.

The surfaces used were prepared by electroplating nickel onto an aluminium substrate to be dissolved later. This technique allows the formation of desired roughness patterns also on the inside wall of a pipe.

The data show an enhancement of the mass transfer rate varying with both flow conditions and surface roughness. At low Reynolds numbers, large roughness elements perform best; as Re is increased, smaller roughnesses give the best results. The data are correlated adequately by the mass transfer similarity function. The highest enhancements reported occur at $e^+ \simeq 10$–15, with the high values exceeding three. A mass transfer efficiency index is proposed which relates the benefit to the cost of increased frictional losses; index values in the range of 2–3 are reported; at unity, the mass transfer gains would equal the frictional losses.

Where comparisons are possible, data agree generally well with published results. Note must be taken of the frequency and shape of the roughness elements which may have a strong influence on results. Important future work, necessary to make progress in understanding flow and mass transfer phenomena, is outlined.

Acknowledgements—Financial support from the Natural Sciences and Engineering Research Council is gratefully acknowledged along with scholarship aid to W. Zhao from the University of Toronto. The authors are grateful to INCO Ltd for their support in supplying the nickel used to make all transfer surfaces.

REFERENCES

1. Nikuradse, T., Laws of flow in rough pipes. *V.D.I. Forschungsheft*, 1933, **361,** Series B, 4; NACA TM 1291, 1950.
2. Dipprey, D. F. and Sabersky, R. H., Heat and momentum transfer in smooth and rough tubes at various Prandtl numbers. *International Journal of Heat and Mass Transfer*, 1963, **6,** 329–253.
3. Dawson, D. A., High Schmidt number mass transfer at rough surfaces. Ph.D. thesis, University of Toronto, 1968.
4. Dawson, D. A. and Trass, O., Mass transfer at rough surfaces. *International Journal of Heat and Mass Transfer*, 1972, **15,** 1317–1336.
5. Tantirige, S. and Trass, O., Mass transfer at geometrically dissimilar rough surfaces. *Canadian Journal of Chemical Engineering*, 1984, **62,** 490–496.
6. Zhao, W., High Schmidt number mass transfer at rough surfaces in pipe flow. Ph.D. thesis, University of Toronto, 1995.
7. Lin, C. S., Denton, E. B., Gaskill, H. S. and Putnam, G. L., Diffusion controlled electrode reactions. *Industrial and Engineering Chemistry*, 1951, **43,** 2136–2143.
8. Pickett, D. and Ong, K. L., The influence of hydrodynamic and mass transfer entrance effects on the operation of a parallel plate electrolytic cell. *Electrochimica Acta*, 1974, **19,** 875–882.
9. Grimanis, M. and Abedian, B., Turbulent mass transfer in rough tubes at high Schmidt numbers. *Physicochemical Hydrodynamics*, 1985, **6,** 775–787.
10. Webb, R. L., Eckert, L. R. G. and Goldstein, R. J., Heat transfer and friction in tubes with repeated rib roughness. *International Journal of Heat and Mass Transfer*, 1971, **14,** 601–617.
11. Gowen, R. A. and Smith, J. W., Turbulent heat transfer from smooth and rough surfaces. *International Journal of Heat and Mass Transfer*, 1968, **11,** 1657–1674.
12. Schlichting, H., *Boundary Layer Theory*, 7th edn. McGraw–Hill, New York, 1979.
13. Treiber, S., Surface characterization and mass transfer at randomly rough surfaces. M.A.Sc. thesis, University of Toronto, 1974.
14. Tantirige, S., Iribarne, A. P., Ojha, M. and Trass, O., The turbulent boundary layer over single V-shaped grooves. *International Journal of Heat and Mass Transfer*, 1994, **37,** 2261–2271.
15. Ojha, M., Hummel, R. L., Cobbold, R. S. C. and Johnston, K. W., Development and evaluation of a high resolution photochromic dye method for pulsatile flow studies. *Journal of Physics: E. Scientific Instruments*, 1988, **21,** 998–1004.
16. Reiss, L. P. and Hanratty, T. J., Measurement of instantaneous rates of mass transfer to a small sink on a wall. *AIChE Journal*, 1962, **8,** 245–247.
17. Kline, S. J., Reynolds, W. C., Schraub, F. A. and Runstadler, P. W., The structure of turbulent boundary layers. *Journal of Fluid Mechanics*, 1967, **30,** 741–773.